Original Article

Institution of MECHANICAL ENGINEERS
Journal of MECHANICAL ENGINEERING SCIENCE

Proc IMechE Part C:
J Mechanical Engineering Science
2014, Vol. 228(13) 2303–2313

DOI: 10.1177/0954406213517871
pic.sagepub.com
SAGE

Modal decoupling control for a double gimbal magnetically suspended control moment gyroscope based on modal controller and feedback linearization method

Xiaocen Chen[1] and Yuan Ren[2]

Abstract

To effectively reject the gyroscopic effects and moving-gimbal effects of the double gimbal magnetically suspended control moment gyroscope (DGMSCMG) and to avoid high control effort, this paper proposes a novel control method based on modal decoupling strategy. Modal controller is employed to realize the modal separation of the translation and rotation modes of the magnetically suspended rotor (MSR). Then the dynamic coupling among the two rotation modes of the MSR system and the two rotational motions of the gimbal servo systems have been decoupled by using differential geometry theory. Dynamic compensation filters have been designed to improve the decoupling performance and the system stability without large control resource. Compared with the existing channel decoupling method, the presented one can not only realize the separate control of stiffness and damping of the MSR but also simplify the control system design significantly. The simulation results verify the effectiveness and superiority of the proposed method.

Keywords

Double gimbal magnetically suspended control moment gyroscope (DGMSCMG), gyroscopic effects, moving-gimbal effects, feedback linearization method, modal decoupling control

Date received: 8 June 2013; accepted: 29 November 2013

Introduction

As the new era puts forward higher demand for the rapid mobility of the spacecraft, control moment gyroscope (CMG) has been becoming the dominating inertial actuator due to its large output torque and long life properties.[1–3] According to the difference of the bearing modes, CMG can be divided into mechanical CMG and magnetically suspended CMG (MSCMG).[4] Compared to the mechanical CMG, MSCMG possesses the priority of zero friction, active vibration suppression, long life span and great potential of high control accuracy.[5–7] According to the different degree-of-freedom (DOF) of the output moment, MSCMG can be classified into single gimbal MSCMG (SGMSCMG) and double gimbal MSCMG (DGMSCMG).[8] In comparison with the SGMSCMG, the DGMSCMG can afford to control 2-DOF which effectively reduces the whole volume and weight of the initial actuator. Above factors make DGMSCMG the ideal actuator for the attitude control of the spacecraft.[9]

However, DGMSCMG is a multivariable, strong coupled system with significant gyroscopic effects and moving-gimbal effects.[9] The control of this dynamic system proves to be a puzzling and challenging issue.[9] Especially the nonlinearities between the inner and the outer gimbal servo systems as well as among the magnetically suspended rotor (MSR) system and the gimbal servo systems make the high-precision and strong-robustness control for the DGMSCMG more complex.[7]

[1]Beijing Institute of Special Electromechanical Technology, The lab of anti-aircraft weapon, Beijing, China
[2]The Department of Space Equipment, The Academy of Equipment, Beijing, China

Corresponding author:
Yuan Ren, The Department of Space Equipment, The Academy of Equipment, No. 92, P. O. Box 3380, HuaiRou District, Beijing 101416, China.
Email: renyuan823@gmail.com

In recent years, a number of methods have been proposed to resolve such issue. The traditional method is cross feedback[10,11] plus compound control based on the angular velocity feedback and given angular acceleration feedforward.[9] On one hand, the cross feedback control method is designed to inhibit the gyroscopic effects. However, this method cannot realize the modal decoupling control between the translation and rotation modes of the MSR. On the other hand, the compound control is designed to inhibit the moving-gimbal effects. Due to the distinction between the given angular acceleration and the actual one, the dynamic properties of the controlled plant are not ideal. Linearization and decoupling (L&D) method has been widely applied in the magnetic bearing (MB) systems,[12–14] such as one DOF MB systems, some simple multiple DOF MB systems. For a SGMSCMG, Fang and Ren[15] prove the system can be linearized and by employing the L&D method based on the current mode, they can successfully decouple and precisely control the SGMSCMG. However, this decoupling strategy is far away from simplicity since all the coupling channels need to be phase-compensated and combined with robust controllers. Especially for the DGMSCMG, this channel decoupling strategy will make the control system quite tedious. Most importantly, this decoupling strategy cannot realize separate adjustment of the stiffness and damping of the MSR,[15] which increases the difficulty of the controller design. Additionally, this decoupling method depends heavily on the system model, deteriorating the system robustness to model errors. Especially for the DGMSCMG, a precise modeling is more difficult than that of the SGMSCMG due to its more complex dynamic coupling and stronger nonlinearity. There is rare literature reporting the high-precision and strong-robustness control of the DGMSCMG. The reason for this may be the difficulty in the feedback linearization caused by the strong coupling and nonlinearity of the system.

This paper is aimed to overcome the shortcomings of the channel decoupling method from a new perspective which combines the modal separation and the feedback linearization decoupling. Modal controller is employed to decouple the translation and rotation modes of the MSR, and the differential geometry method is adopted to achieve the exact linearization and decoupling among the 4-DOF rotation motions of the DGMSCMG. The main contribution of this paper lies in that the proposed control strategy can realize high-precision and strong-robustness decoupling control for the DGMSCMG without high control effort.

The remainder of this paper is organized as follows: In "Modeling and analysis of the characteristics of the DGMSCMG" section, we construct the model of the DGMSCMG and analyze the characteristics of the dynamic system from the perspective of modal analysis. Next, an L&D method based on the differential geometry theory is introduced to decouple the 4-DOF rotation modes of the DGMSCMG completely in "Modal decoupling control based on modal separation and rotation modes decoupling" section. "Simulation results" section conducts the comparative simulations to testify the decoupling performance with the proposed method. Follow on, "Conclusion" section concludes this paper.

Modeling and analysis of the characteristics of the DGMSCMG

Modeling of the DGMSCMG

The overall structure and coordinates of the DGMSCMG and the MSR system are shown in Figure 1 and Figure 2, respectively.

As shown in Figure 1, θ_g and θ_j represent the rotational angles of the inner gimbal and the outer gimbal servo systems, respectively, and Ω is rotor speed. In Figure 2, O is the geometric center of the MB stator; X, Y and Z axes form the generalized coordinates of the rotor position; f_x and f_y are the magnetic forces in the X and Y directions, respectively; f_{ax}, f_{ay}, f_{bx} and f_{by} are the magnetic forces along the radial magnetic coordinates Ax, Ay, Bx and By; p_x and p_y are the output torques in the X and Y directions, respectively; and α and β are the rotational angles about the X and Y axes, respectively.

The model of the DGMSCMG can be expressed as follows:

$$
\begin{cases}
m\ddot{x} = f_{ax} + f_{bx} \\
m\ddot{y} = f_{ay} + f_{by} \\
J_{rr}\left(\frac{\sqrt{2}}{2}\ddot{\theta}_j\cos\theta_g - \frac{\sqrt{2}}{2}\dot{\theta}_j\dot{\theta}_g\sin\theta_g + \frac{\sqrt{2}}{2}\ddot{\theta}_g + \ddot{\alpha}\right) + H_{rz}\left(\frac{\sqrt{2}}{2}\dot{\theta}_j\cos\theta_g - \frac{\sqrt{2}}{2}\dot{\theta}_g + \dot{\beta}\right) = p_x = l_m(f_{by} - f_{ay}) \\
J_{rr}\left(\frac{\sqrt{2}}{2}\ddot{\theta}_j\cos\theta_g - \frac{\sqrt{2}}{2}\dot{\theta}_j\dot{\theta}_g\sin\theta_g - \frac{\sqrt{2}}{2}\ddot{\theta}_g + \ddot{\beta}\right) - H_{rz}\left(\frac{\sqrt{2}}{2}\dot{\theta}_j\cos\theta_g + \frac{\sqrt{2}}{2}\dot{\theta}_g + \dot{\alpha}\right) = p_y = l_m(f_{ax} - f_{bx}) \\
J_{gx}\ddot{\theta}_g - (J_{gz} - J_{gy})\dot{\theta}_j^2\sin\theta_g\cos\theta_g + \frac{\sqrt{2}}{2}(p_x - p_y) = p_{gx} \\
J_{gy}(\ddot{\theta}_j\cos\theta_g - \dot{\theta}_j\dot{\theta}_g\sin\theta_g) - (J_{gx} - J_{gz})\dot{\theta}_j\dot{\theta}_g\sin\theta_g + \frac{\sqrt{2}}{2}(p_x + p_y) = p_{gy} \\
-J_{gz}\ddot{\theta}_j\sin\theta_g + (J_{gy} - J_{gx} - J_{gz})\dot{\theta}_j\dot{\theta}_g\cos\theta_g = p_{gz} \\
J_{jy}\ddot{\theta}_j + p_{gy}\cos\theta_g - p_{gz}\sin\theta_g = p_{jy}
\end{cases}
\tag{1}
$$

where m is the mass of the rotor, J_{rr}, J_z are moments of inertia along the radial and axial magnetic coordinates of the MSR, respectively, J_{gx}, J_{gy}, J_{gz} are moments of inertia along the coordinates of the inner gimbal rate-servo system; J_{jy} is moment of inertia in the output torque direction of the outer gimbal rate-servo system, $P_{gx} = k_{igx} i_{gx}$, $P_{jy} = k_{ijy} i_{jy}$, $H_{rz} = J_z \Omega$, H_{rz} is angular momentum of the MSR system; k_{igx} and k_{ijy} are the current stiffness, while P_{gx} and P_{jy} demonstrate the output torques of the inner and outer gimbal rate-servo system, respectively.

As for the MSR system, the magnetic force can be formulated by a variable operating-point linearization method.[15] That is, it can be linearized as

$$f_\lambda = k_{i\lambda} i_\lambda + k_{h\lambda} h_\lambda (\lambda = ax, ay, bx, by) \tag{2}$$

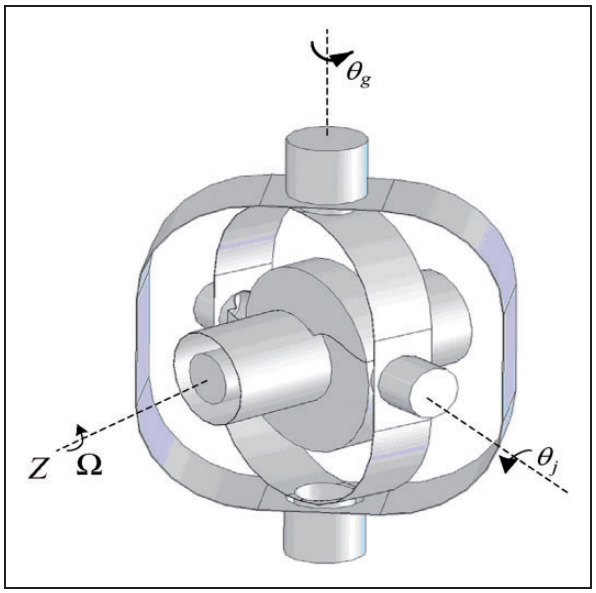

Figure 1. Structure and coordinates of the double gimbal magnetically suspended control moment gyroscope (DGMSCMG).

where $k_{i\lambda}$, $k_{h\lambda}$, h_λ and i_λ are the current-force-factor (current stiffness), the displacement-force-factor (position stiffness),[15] the linear displacement and the winding current of channel $\lambda (\lambda = ax, ay, bx, by)$, and $[i_{ax}, i_{bx}, i_{ay}, i_{by}]^T$ form the MB actuator coordinates, respectively. i_{ax}, i_{bx}, i_{ay}, i_{by}, i_{gx} and i_{jy} are the control inputs of the DGMSCMG system.

Analysis of the characteristics of the DGMSCMG

In the generalized coordinate system of the rotor position, define $i_{\lambda t}$ the translation current and $i_{\lambda r}$ the rotation current of MBs $(\lambda = ax, ay, bx, by)$, which generate the translation and rotation motions of the MSR, respectively. Then we have $i_\lambda = i_{\lambda t} + i_{\lambda r}$, $k_{iax} i_{axt} = k_{ibx} i_{bxt}$, $k_{iay} i_{ayt} = k_{iby} i_{byt}$, $k_{iax} i_{axr} = -k_{ibx} i_{bxr}$ and $k_{iay} i_{ayr} = -k_{iby} i_{byr}$.

Accordingly, the dynamical equations of the translation and rotation modes of the MSR can be formulated as

$$\begin{cases} m\ddot{x} = f_{ax} + f_{bx} = 2k_{iax} i_x + 2k_{hax} x - \Delta k_{hx} h_{bx} \\ m\ddot{y} = f_{ay} + f_{by} = 2k_{iby} i_y + 2k_{hby} y - \Delta k_{hy} h_{ay} \\ p_x = (f_{by} - f_{ay}) l_m = 2l_m k_{iby} i_\beta + 2l_m^2 k_{hby} \alpha + l_m \Delta k_{hy} h_{ay} \\ p_y = (f_{ax} - f_{bx}) l_m = 2l_m k_{iax} i_\alpha + 2l_m^2 k_{hax} \beta + l_m \Delta k_{hx} h_{bx} \end{cases} \tag{3}$$

where l_m denotes the distance from the acting point of the magnetic force along the radial magnetic coordinates to the geometric center O, $h_{ax} = x + l_m \beta$, $h_{bx} = x - l_m \beta$, $h_{ay} = y - l_m \alpha$, $h_{by} = y + l_m \alpha$, $i_x = i_{axt} = k_{ibx} i_{bxt} / k_{iax}$, $i_y = i_{byt} = k_{iay} i_{ayt} / k_{iby}$, $i_a = i_{axr} = -k_{ibx} i_{bxr} / k_{iax}$, $i_\beta = i_{byr} = -k_{iay} i_{ayr} / k_{iby}$, $\Delta k_{hx} = k_{hax} - k_{hbx}$, $\Delta k_{hy} = k_{hby} - k_{hay}$. $[i_x, i_\alpha, i_y, i_\beta]^T$ constitute the modal coordinates, and $[x, \beta, y, \alpha]^T$ form the generalized coordinates of the rotor position.

Then the coordinate transformation from the modal coordinates to MB actuator coordinates

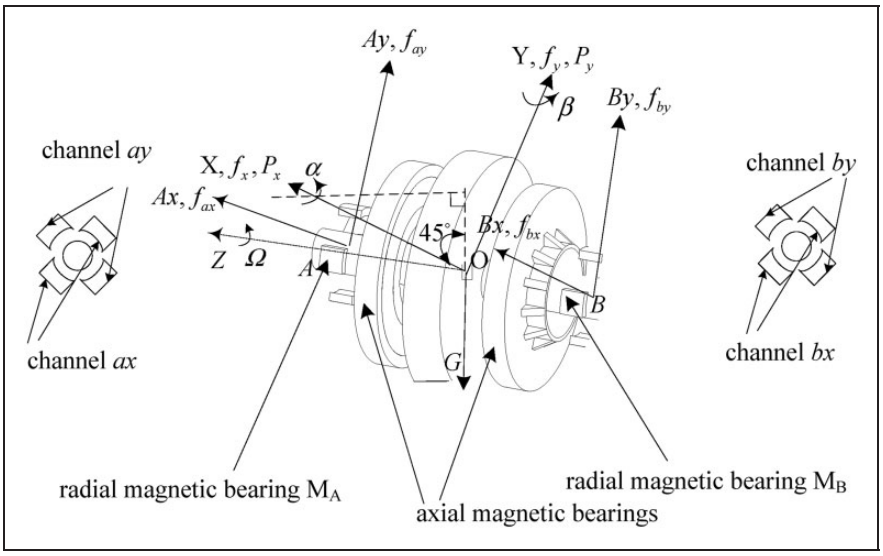

Figure 2. Structure and coordinates of the magnetically suspended rotor (MSR) system.

can be yielded

$$\begin{cases} i_{ax} = i_x + i_\alpha \\ i_{bx} = k_{iax}/k_{ibx}(i_x - i_\alpha) \\ i_{ay} = k_{iby}/k_{iay}(i_y - i_\beta) \\ i_{by} = i_y + i_\beta \end{cases} \tag{4}$$

Combining equations (1) and (3) yields, in the generalized coordinate system of the rotor position, there are no couplings between the translation and rotation motions of the MSR if and only if $\Delta k_{hx} = \Delta k_{hy} \equiv 0$, that is, the two channels with the same translation DOF always have the same displacement-force-factors. Unfortunately this does not happen in most practical situations due to the errors caused by manufacturing, fabrication, material and so on. In other words, there also exist dynamic coupling between the translation and rotation modes of the MSR system.

According to equation (1), it is obvious that there are strong dynamic coupling among α, β, θ_g and θ_j. For the sake of convenience, both the 2-DOF rotation modes and the 2-DOF rotation motions of the inner and the outer gimbal servo system are called 4-DOF rotation modes of the DGMSCMG. Accordingly, as for the practical DGMSCMG system, there are dynamic couplings not only among the 4-DOF rotation modes of the DGMSCMG, but also between the 2-DOF translation modes and 4-DOF rotation modes of the DGMSCMG.

Now that the rotation mode couplings among α, β, θ_g and θ_j are the essential cause for the gyro effects and moving-gimbal effects, which influence both the stability and the control precision. And the couplings between the 2-DOF translation and 2-DOF rotation motions of the MSR inhibit the separate control of the stiffness and damping of the MSR, which is the key factor influencing the system stability. Thus the precise linearization decoupling control among the 4-DOF rotation modes and the modal separation of the MSR are reasonable and necessary.

Moreover, the analytical solutions of the output torques of the two gimbal rate-servo systems can be yielded as follows:

$$\begin{aligned} p_{gx} = {} & J_{gx}\ddot{\theta}_g + (J_{gy} - J_{gz})\dot{\theta}_j^2 \sin\theta_g \cos\theta_g \\ & + J_{rr}\left[\frac{\sqrt{2}}{2}(\ddot{\alpha} - \ddot{\beta}) + \ddot{\theta}_g\right] + H_{rz}\left(\dot{\theta}_j \cos\theta_g + \frac{\sqrt{2}}{2}(\dot{\alpha} + \dot{\beta})\right) \\ p_{jy} = {} & \left(J_{jy} + J_{gy}\cos^2\theta_g + J_{gz}\sin^2\theta_g + J_{rr}\cos\theta_g^2\right)\ddot{\theta}_j \\ & + J_{rr}\left[\frac{\sqrt{2}}{2}(\ddot{\alpha} + \ddot{\beta})\cos\theta_g - \dot{\theta}_j\dot{\theta}_g \sin\theta_g \cos\theta_g\right] \\ & - H_{rz}\left[\frac{\sqrt{2}}{2}(\dot{\alpha} - \dot{\beta}) + \dot{\theta}_g\right]\cos\theta_g \\ & - 2(J_{gy} - J_{gz})\dot{\theta}_g\dot{\theta}_j \sin\theta_g \cos\theta_g \end{aligned} \tag{5, 6}$$

From equations (5) and (6), we can discover that the rotation modes of the MSR system aggravate greatly the nonlinearity and coupling effects among the MSR system and the two gimbal rate-servo systems, which accounts for the stronger moving-gimbal effects of the DGMSCMG than that of the SGMSCMG.

To sum up, for realizing the high-precision and strong-robustness control of the DGMSCMG, we can just pay attention to the modal decoupling based on modal separation and rotation modes decoupling.

Modal decoupling control based on modal separation and rotation modes decoupling

The goal of the modal control is to realize the separate control between the translation and rotation modes of the MSR. To achieve this objective, the negative stiffness of the MB needs to be cancelled, which is performed in the controller by adding an equal and opposite stiffness to the MB command signal.[16] Control of the translation motions is relatively simple, and only the rotation motions exhibit speed-dependent gyroscopic effects and moving-gimbal effects. Consequently, the traditional modal proportional-integral-derivative (PID) controllers are retained to realize the translation control. And the 4-DOF rotation modes decoupling control of the DGMSCMG based on differential geometry theory is further developed.

Rotation modes decoupling control based on differential geometry theory

According to the differential geometry theory, the steps of finding the suitable feedback systems can be described as Figure 3.

As for the rotation modes of the DGMSCMG, the state variable $\boldsymbol{x}$, input variable $\boldsymbol{u}$ and output variable $\boldsymbol{y}$ can be defined as follows:

$$\begin{aligned} \boldsymbol{x} &= \begin{bmatrix} x_1 & x_2 & x_3 & x_4 & x_5 & x_6 & x_7 & x_8 \end{bmatrix}^T \\ &= \begin{bmatrix} \alpha & \beta & \theta_g & \theta_j & \dot{\alpha} & \dot{\beta} & \dot{\theta}_g & \dot{\theta}_j \end{bmatrix}^T \end{aligned}$$

$$\boldsymbol{u} = \begin{bmatrix} u_1 & u_2 & u_3 & u_4 \end{bmatrix}^{\mathrm{T}} = \begin{bmatrix} i_\alpha & i_\beta & i_{gx} & i_{jy} \end{bmatrix}^T$$

$$\boldsymbol{y} = \begin{bmatrix} y_1 & y_2 & y_3 & y_4 \end{bmatrix}^{\mathrm{T}} = \begin{bmatrix} \alpha & \beta\theta_g & \theta_j \end{bmatrix}^T$$

The dynamical equations of the DGMSCMG can be converted into the state space model of the affine nonlinear system:

$$\begin{cases} \dot{\boldsymbol{x}} = f(\boldsymbol{x}) + g(\boldsymbol{x})\boldsymbol{u} \\ \boldsymbol{y} = h(\boldsymbol{x}) \end{cases} \tag{7}$$

where the expression of $f(\boldsymbol{x})$ is given in Appendix 1.

$$h(\boldsymbol{x}) = \begin{bmatrix} x_1 & x_2 & x_3 & x_4 \end{bmatrix}^T \tag{8}$$

$$g_1(\boldsymbol{x})=\begin{bmatrix} 0 \\ 0 \\ 0 \\ 0 \\ \dfrac{k_{iax}l_m\cos x_3^2}{\lambda_2}-\dfrac{k_{iax}l_m}{J_{gx}} \\ \dfrac{2k_{iax}l_m}{J_{rr}}+\dfrac{k_{iax}l_m\cos x_3^2}{\lambda_2}+\dfrac{k_{iax}l_m}{J_{gx}} \\ \dfrac{\sqrt{2}k_{iax}l_m}{J_{gx}} \\ \dfrac{-\sqrt{2}k_{iax}l_m\cos x_3}{\lambda_2} \end{bmatrix},$$

$$g_2(\boldsymbol{x})=\begin{bmatrix} 0 \\ 0 \\ 0 \\ 0 \\ \dfrac{2k_{iby}l_m}{J_{rr}}+\dfrac{k_{iby}l_m\cos x_3^2}{\lambda_2}+\dfrac{k_{iby}l_m}{J_{gx}} \\ \dfrac{k_{iby}l_m\cos x_3^2}{\lambda_2}-\dfrac{k_{iby}l_m}{J_{gx}} \\ -\dfrac{\sqrt{2}k_{iby}l_m}{J_{gx}} \\ \dfrac{-\sqrt{2}k_{iby}l_m\cos x_3}{\lambda_2} \end{bmatrix},$$

$$g_3(\boldsymbol{x})=\begin{bmatrix} 0 \\ 0 \\ 0 \\ 0 \\ \dfrac{-\sqrt{2}k_{igx}}{2J_{gx}} \\ \dfrac{\sqrt{2}k_{igx}}{2J_{gx}} \\ \dfrac{k_{igx}}{J_{gx}} \\ 0 \end{bmatrix},\quad g_4(\boldsymbol{x})=\begin{bmatrix} 0 \\ 0 \\ 0 \\ 0 \\ \dfrac{-\sqrt{2}k_{ijy}\cos x_3}{2\lambda_2} \\ \dfrac{-\sqrt{2}k_{ijy}\cos x_3}{2\lambda_2} \\ 0 \\ \dfrac{k_{ijy}}{\lambda_2} \end{bmatrix} \tag{9}$$

where $\lambda_2 = J_{jy} + J_{gy}\cos x_3^2 + J_{gz}\sin x_3^2$.

On the basis of the differential geometry theory,[17] we have

$$L_{g_i}h_j(\boldsymbol{x}) = 0\,(i,j=1,2,3,4) \tag{10}$$

$$\boldsymbol{A}(x)=\begin{bmatrix} L_{g_1}L_fh_1(\boldsymbol{x}) & L_{g_2}L_fh_1(\boldsymbol{x}) & L_{g_3}L_fh_1(\boldsymbol{x}) & L_{g_4}L_fh_1(\boldsymbol{x}) \\ L_{g_1}L_fh_2(\boldsymbol{x}) & L_{g_2}L_fh_2(\boldsymbol{x}) & L_{g_3}L_fh_2(\boldsymbol{x}) & L_{g_4}L_fh_2(\boldsymbol{x}) \\ L_{g_1}L_fh_3(\boldsymbol{x}) & L_{g_2}L_fh_3(\boldsymbol{x}) & L_{g_3}L_fh_3(\boldsymbol{x}) & L_{g_4}L_fh_3(\boldsymbol{x}) \\ L_{g_1}L_fh_4(\boldsymbol{x}) & L_{g_2}L_fh_4(\boldsymbol{x}) & L_{g_3}L_fh_4(\boldsymbol{x}) & L_{g_4}L_fh_4(\boldsymbol{x}) \end{bmatrix}$$

$$=\begin{bmatrix} \dfrac{k_{iax}l_m\cos x_3^2}{\lambda_2}-\dfrac{k_{iax}l_m}{J_{gx}} & \dfrac{2k_{iby}l_m}{J_{rr}}+\dfrac{k_{iby}l_m\cos x_3^2}{\lambda_2}+\dfrac{k_{iby}l_m}{J_{gx}} & \dfrac{-\sqrt{2}k_{igx}}{2J_{gx}} & \dfrac{-\sqrt{2}k_{ijy}\cos x_3}{2\lambda_2} \\ \dfrac{2k_{iax}l_m}{J_{rr}}+\dfrac{k_{iax}l_m\cos x_3^2}{\lambda_2}+\dfrac{k_{iax}l_m}{J_{gx}} & \dfrac{k_{iby}l_m\cos x_3^2}{\lambda_2}-\dfrac{k_{iby}l_m}{J_{gx}} & \dfrac{\sqrt{2}k_{igx}}{2J_{gx}} & \dfrac{-\sqrt{2}k_{ijy}\cos x_3}{2\lambda_2} \\ \dfrac{\sqrt{2}k_{iax}l_m}{J_{gx}} & -\dfrac{\sqrt{2}k_{iby}l_m}{J_{gx}} & \dfrac{k_{igx}}{J_{gx}} & 0 \\ \dfrac{-\sqrt{2}k_{iax}l_m\cos x_3}{\lambda_2} & \dfrac{-\sqrt{2}k_{iby}l_m\cos x_3}{\lambda_2} & 0 & \dfrac{k_{ijy}}{\lambda_2} \end{bmatrix} \tag{11}$$

Then the determinant of $\boldsymbol{A}(\boldsymbol{x})$is

$$\det(\boldsymbol{A}(\boldsymbol{x})) = -\frac{4l_m^2k_{iax}k_{iby}k_{igx}k_{ijy}}{J_{rr}J_{gx}\lambda_2}\left(\frac{1}{J_{rr}}+\frac{1}{J_{rr}J_{gx}}+\frac{\cos x_3^2}{\lambda_2}\right)\neq 0 \tag{12}$$

As the matrix $\boldsymbol{A}(\boldsymbol{x})$ is nonsingular, it can be drawn that the system (7) is of vector relative degree $\{2,2,2,2\}$, and $8 = 2 + 2 + 2 + 2$ is equal to the system dimension. Accordingly, the system can be full state feedback linearized.

Define new variables to substitute for the second derivatives of the original output variables. Namely,

$$\boldsymbol{v}=\begin{bmatrix} v_1 & v_2 & v_3 & v_4 \end{bmatrix}^T=\begin{bmatrix} \ddot{y}_1 & \ddot{y}_2 & \ddot{y}_3 & \ddot{y}_4 \end{bmatrix}^T.$$

The nonlinear feedback linearization control law can be described as

$$\boldsymbol{u} = \boldsymbol{A}^{-1}(\boldsymbol{x})(\boldsymbol{v}-\boldsymbol{B}(\boldsymbol{x})) \tag{13}$$

where $\boldsymbol{B}(\boldsymbol{x})$ is given in Appendix 1. Combining the analytical formulations of $\boldsymbol{A}(\boldsymbol{x})$ and $\boldsymbol{B}(\boldsymbol{x})$ yields the feedback linearization control arithmetic as follows:

$$u_1=\frac{1}{2k_{iax}l_m}\left[J_{rr}\left(\frac{\sqrt{2}}{2}v_4\cos x_3-\frac{\sqrt{2}}{2}x_7x_8\sin x_3-\frac{\sqrt{2}}{2}v_3+v_2\right)-H_{rz}\left(\frac{\sqrt{2}}{2}x_8\cos x_3+\frac{\sqrt{2}}{2}x_7+x_5\right)-2k_{hax}l_m^2x_2\right] \tag{14}$$

$$u_2=\frac{1}{2k_{iby}l_m}\left[J_{rr}\left(\frac{\sqrt{2}}{2}v_4\cos x_3-\frac{\sqrt{2}}{2}x_7x_8\sin x_3+\frac{\sqrt{2}}{2}v_3+v_1\right)+H_{rz}\left(\frac{\sqrt{2}}{2}x_8\cos x_3-\frac{\sqrt{2}}{2}x_7+x_5\right)-2k_{hby}l_m^2x_1\right] \tag{15}$$

$$u_3 = \frac{1}{k_{igx}}\left[J_{gx}v_3 - \lambda_3 + J_{rr}\left[\frac{\sqrt{2}}{2}(v_1 - v_2) + v_3\right] + H_{rz}\left(x_8\cos x_3 + \frac{\sqrt{2}}{2}(x_6 + x_5)\right)\right] \tag{16}$$

$$u_4 = \frac{1}{k_{ijy}} \times \left[\lambda_2 v_4 - H_{rz}\left[\frac{\sqrt{2}}{2}(x_5 - x_6) + x_7\right]\cos x_3 - \lambda_1 + J_{rr} \times \left[\frac{\sqrt{2}}{2}(v_1 + v_2) + (v_4\cos x_3 - x_7 x_8 \sin x_3)\right]\cos x_3\right] \tag{17}$$

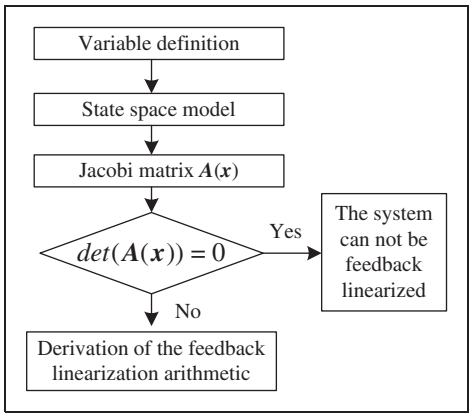

Figure 3. The steps of finding the suitable feedback systems.

Compared with the channel decoupling method, we just need to deal with the decoupling issue of the dynamic system with 4-DOF instead of 6-DOF, which greatly simplifies the feedback linearization arithmetic.

Realization of the proposed control strategy

The decoupled plants are often combined with robust controllers since the remaining coupling and nonlinearity always exists in practice.[18] Two-DOF inner modal controller (IMC) is chosen in this paper due to its exciting robustness and simplicity,[15] where $G_c(s) = \frac{s^2}{(\varepsilon_2 s+1)^2-1}$, $G_f(s) = \frac{(\varepsilon_2 s+1)^2}{(\varepsilon_1 s+1)^2}$. Besides, as for the current mode feedback linearization method, phase compensation is necessary to the decoupled subsystems due to phase lag of the control system,[19] especially for the nutation mode of the MSR system.[20] As for the gimbal servo system, note that the phase lag is smaller than that of the rotation modes of the MSR system,[21] and it has little influence on the system stability. Accordingly, only the phase compensations for the two rotation modes of the MSR system are performed.

Figure 4 shows the schematic of the proposed controller based on modal decoupling strategy, where $G_p(s)$ is the phase compensation filter, $G_f(s)$ and $G_c(s)$ constitute the 2-DOF IMC,[14] $G_t(s)$ is the translation PID controller, Δi_{ax}, Δi_{bx}, Δi_{ay} and Δi_{by} are the compensation currents to cancel the negative stiffness of the corresponding channel, and $\Delta i_{ax} = \frac{k_{hax}h_{ax}}{k_{iax}}$, $\Delta i_{bx} = \frac{k_{hbx}h_{bx}}{k_{ibx}}$, $\Delta i_{ay} = \frac{k_{hay}h_{ay}}{k_{iay}}$ and $\Delta i_{by} = \frac{k_{hby}h_{by}}{k_{iby}}$.

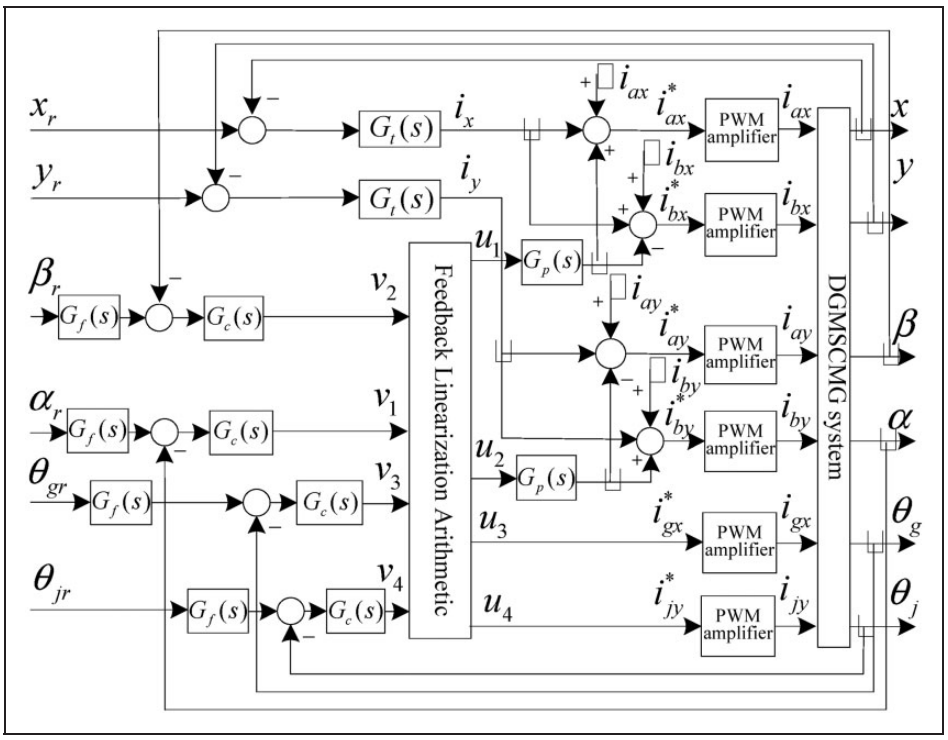

Figure 4. Schematic of the proposed controller based on modal control and feedback linearization method.

Then the controller outputs, i.e. the reference currents of the DGMSCMG can be yielded

$$\begin{cases} i_{ax}^* = i_x + u_1 G_p(s) + \Delta i_{ax} \\ i_{bx}^* = i_x - u_1 G_p(s) + \Delta i_{bx} \\ i_{ay}^* = i_y - u_2 G_p(s) + \Delta i_{ay} \\ i_{by}^* = i_y + u_2 G_p(s) + \Delta i_{by} \\ i_{gx}^* = u_3 \\ i_{jy}^* = u_4 \end{cases} \quad (18)$$

Compared with the channel decoupling method, the number of the combined robust controllers is reduced from 6 to 4, and the number of the phase compensation filters is reduced from 4 to 2. Accordingly, the computational costs can be greatly reduced as well the control accuracy and stability of the MSR system can be improved since little computer resource can reduce the system delay. Most importantly, the proposed method contributes to improving the system robustness against the model errors because the translation controller does not depend heavily on the precise model any more. That is, the robustness of the translation motions can be greatly improved by the proposed strategy. Additionally, as the two modes have their respective performance index, the channel decoupling method has some difficulty in satisfying their performances simultaneously. Compared to the cross feedback plus compound control and channel decoupling control methods, the proposed one can achieve this goal since it can realize the separate control of the stiffness and damping of the MSR system, which is also conductive to improving the system stability and convenience of the controller design. To sum up, the proposed method can cover the shortage of the traditional ones, contributing to the high-precision and strong-robustness control of the DGMSCMG without high control effort.

Simulation results

In this section, we conduct the comparative simulations between the channel decoupling method and the proposed one to verify the satisfactory decoupling effect and high control accuracy as well as strong robustness with the new method.

Simulation conditions

To compare the controller performances fairly, both the two methods employ the same 2-DOF IMC and the same phase compensation filter with

$$G_p(s) = \frac{4s^2 + 9100s + 1.1e7}{0.2s^2 + 7100s + 1.15e7}$$

The system parameters of the DGMSCMG and the main controller coefficients are shown in Tables 1 and 2, respectively.

Table 1. System parameters of the DGMSCMG.

Parameter (unit)	Numerical value	Parameter (unit)	Numerical value
m (kg)	15	J_{rr} (kg m^2)	0.062
l_m (m)	0.06253	J_z (kg m^2)	0.1019
k_{iax} (N/A)	350	k_{hax} (N/m)	8.5e5
k_{ibx} (N/A)	330	k_{hbx} (N/m)	8.3e5
k_{iay} (N/A)	365	k_{hay} (N/m)	8.6e5
k_{iby} (N/A)	342	k_{hby} (N/m)	8.2e5
J_{gx} (kg m^2)	0.098	J_{gy} (kg m^2)	0.297
k_{igx} (N/A)	0.84	J_{gz} (kg m^2)	0.293
k_{ijy} (N/A)	0.84	J_{jy} (kg m^2)	0.7224

Table 2. Main coefficients of the controllers.

Parameter	Value	Parameter	Value
k_{am}	2.0	i_c	10
ε_1	0.007 (0.005)	ε_2	0.002
k_p	0.008	k_f	0.0045

In Table 2, k_{am} and i_c are the proportional and feedback coefficients of the current-loop controller for the MSR system, respectively, ε_1 and ε_2 are the parameters of the IMC, k_p and k_f are the current-loop proportional and feedback coefficients of the gimbal servo systems, respectively.

To demonstrate the influence of control system delay on system performance, control system delay is considered in simulation. Note that the channel decoupling method consumes larger computing resource, which inevitably results in larger control system delay. Suppose the channel decoupling method and the proposed one have 150 μs and 250 μs computation delay, respectively, they are simulated by a delay unit with 150 μs and 250 μs in simulation.

Decoupling and tracking performances

Simulation conditions: under the rated rotor speed 20,000 r/min, at $t = 0.1$ s, the translation mode of the MSR system x receives the step signal instruction with the amplitude of 50 μm. Then at $t = 0.5$ s, the rotation mode of the MSR system α receives the sinusoidal signal instruction with the amplitude of 0.02°, and the angular frequency of which is 4π rad/s. Figure 5 reveals the simulation results. The real (red) and dotted (blue) lines delegate the tracking curves of the proposed method and the channel decoupling one, respectively.

According to Figure 5, we can discover that when concerned with the channel decoupling method, the tracking curves of the whole system are unexciting. At $t = 0.1$ s, when the translation mode of the MSR

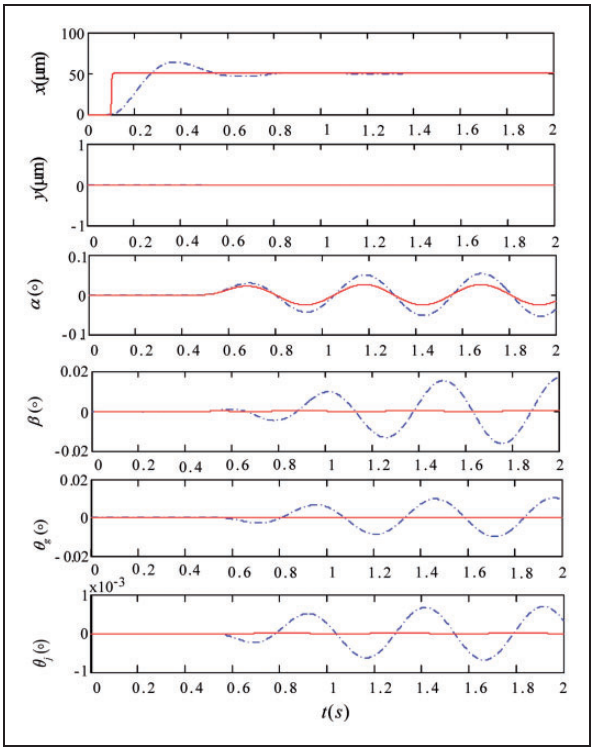

Figure 5. Comparison of decoupling effect.

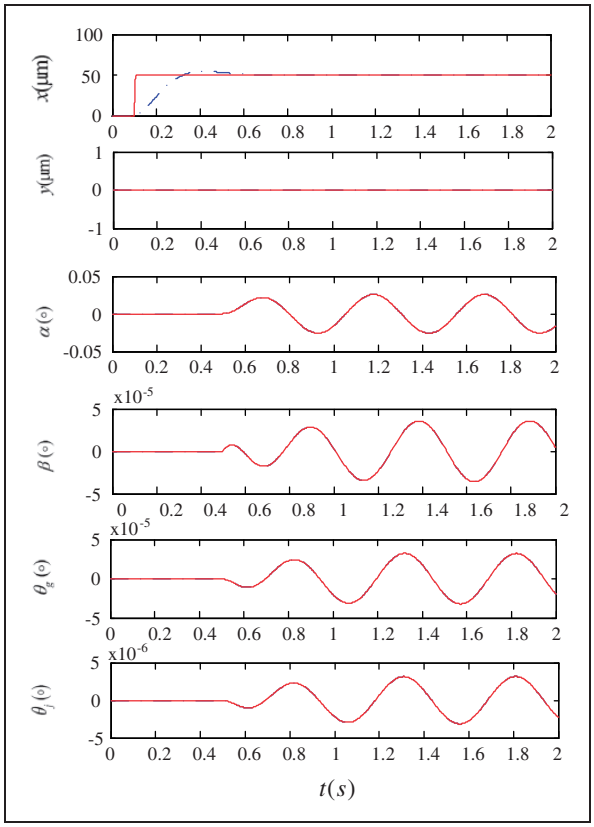

Figure 6. Comparative simulation results between the traditional and the proposed methods with the same time delay.

system x receives the step signal instruction, it does not adapt to the input signal quickly, instead, its response speed is quite low and the settling time is quite long which is up to about 0.8 s. At $t = 0.5$ s, as soon as the rotation mode of the MSR system α receives the sinusoidal signal, there appears overshoot in the tracking curve with the amplitude of about 0.03°, meanwhile, the coupling effects are distinct not only between the two rotation modes of the MSR system but also among the MSR system and the two gimbal rate-servo systems. The amplitude of the tracking curve of rotation mode β reaches 0.02°, and that of the inner gimbal rate-servo system is about 0.01°.

However, when it comes to the proposed method, the tracking curves of the whole system are satisfactory. The response speed is quick, and there exits no overstrike in the tracking curve of the rotation mode α, as well as the coupling effect is little. All of these are conducive to the high precision control of the dynamic system.

The large computational costs the existing method brings about result in the system delay which deteriorates the decoupling accuracy. To verify this point, we carry out the comparative simulations between the proposed method and the existing one after reducing the delay time from 250 μs to 150 μs, That is, the two methods now have the same computation delay. The simulation conditions are identical with that above. Figure 6 demonstrates the simulation results. Also the real and dotted lines represent the proposed method and the channel decoupling method.

From Figure 6, we can summarize that after removing the extra delay link in the dynamic system adopting the traditional method, the tracking curves of the two strategies have much in common. When the rotation mode of the MSR system α receives the sinusoidal signal at $t = 0.5$ s, its tracking curve adapts to the input instruction quickly without any overshoot. Simultaneously, the coupling effects among the MSR system and the two gimbal rate-servo systems as well as the two rotation modes of the MSR system are weakened sharply to the extent of 10^{-5} order of magnitude.

The results confirm the point that the channel decoupling method introduces the excessive system delay, which results in the poor decoupling performance. This coincides with the analysis above. In theory, this can be alleviated to some extent by increasing the phase compensation value. However, this inevitably results in extra system noise in practice.

Modal separation characteristics and robustness to model errors

From Figure 6, it can be found that, as for the channel decoupling method, even with the same time delay, the step response of the translation mode x is slower than that of the proposed method. To overcome the weakness, we decrease ε_1 from 0.007 to 0.005 as for the channel decoupling method. Simultaneously,

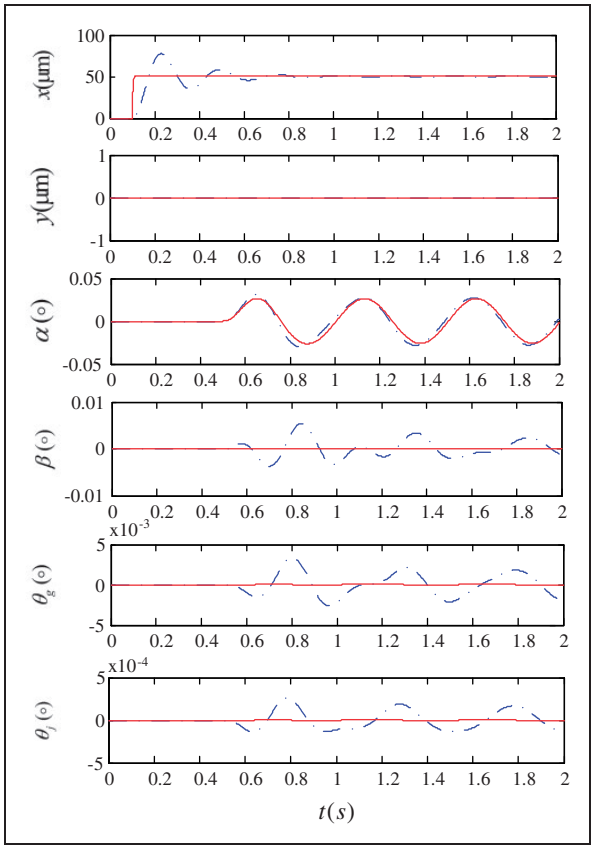

Figure 7. Decentralized control of the translation and rotation modes effect comparison.

to prove the robustness to the model errors of the proposed method, parameter variations are imposed to the system. At $t = 0.5$ s, assume that k_{iax} decreases by 1% and k_{hby} increases by 1%. Figure 7 shows the comparative simulation results.

Compared Figure 7 with Figure 6, it turns out that though the response speed of x is quickened, the tracking curve appears larger overshoot compared to the case that $\varepsilon_1 = 0.007$ and the transient time is still quite long which go against the objective of high precision and high-stability control. The simulation results demonstrate that the channel decoupling method cannot live up to the expectations of making the separate adjustment of the stiffness and dimpling of the MSR system.

According to Figures 5 and 6, as for the proposed method, the parameter variation does not introduce obvious disturbance into the system. On the contrary, they result in evident disturbances and couplings on the four rotation modes of the DGMSCMG when employing the channel decoupling method. This demonstrates that, compared with the channel decoupling method, the robustness of the rotation modes has been greatly improved by the proposed method. All of these simulation results are in accordance with the analysis in "Modal decoupling control based on modal separation and rotation modes decoupling" section.

Conclusion

To resolve the disadvantages of the existing decoupling control methods for a DGMSCMG, a novel control method based on modal separation and rotation modes decoupling is proposed in this paper. Analysis and simulation results demonstrate that the proposed method has exciting advantages compared with the channel decoupling method:

1. has higher control precision and better decoupling performance;
2. can realize the separate control of stiffness and damping of the MSR;
3. has stronger robustness against model errors and parameter variations;
4. can simplify greatly the controller design.

To sum up, the presented method can effectively reject the gyroscopic effects and moving-gimbal effects of the DGMSCMG without high control effort, realizing its high-precision and strong-robustness control.

Conflict of interest

None declared.

Funding

This work was supported in part by the National Basic Research Program of China, and in part by the National Science Foundation of China.

References

1. Bhat SP and Tiwari PK. Controllability of spacecraft attitude using control moment gyroscopes. *IEEE Trans Automat Control* 2009; 54(3): 585–590.
2. Carpenter MD and Peck MA. Reducing base reactions with gyroscopic actuation of space-robotic systems. *IEEE Trans Robot* 2009; 25(6): 1262–1270.
3. Carpenter MD and Peck MA. Dynamics of a high-agility, low-power imaging payload. *IEEE Trans Robot* 2008; 24(3): 666–675.
4. Thornton B, Ura T, Nose Y, et al. Zero-G class underwater robots: unrestricted attitude control using control moment gyros. *IEEE J Ocean Eng* 2007; 32(3): 565–583.
5. Tang J, Liu B and Sam GS. Suppression of vibration caused by residual unbalance of rotor for magnetically suspended flywheel. *J Vib Control* In press; DOI: 1077546312449643.
6. Liu G, Fang J and Liu J. Research progress on the application of high-speed brushless DC motor in magnetically suspended inertial actuator. *Meas Control* 2008; 41(3): 88–91.
7. Ji JC, Hansen CH and Zander AC. Nonlinear dynamics of magnetic bearing systems. *J Intel Mater Syst Struc* 2008; 19(12): 1471–1491.
8. Fang J, Zheng S and Hang B. AMB vibration control for structural resonance of double-gimbal control moment gyro with high-speed magnetically suspended rotor. *IEEE/ASME Trans Mechatron* 2013; 18(1): 32–43.

9. Wei T, Fang J and Liu Z. Moving-gimbal effects compensation of double gimbal magnetically suspended control moment gyroscope based on compound control. *J Mech Eng* 2010; 46(2): 160–165.
10. Ahrens M, Kucera L and Larsonneur R. Performance of a magnetically suspended flywheel energy storage device. *IEEE Trans Control Syst Technol* 1996; 4(5): 494–502.
11. Brown GV, Kascak A, Jansen RH, et al. Stabilizing gyroscopic modes in magnetic-bearing-supported flywheels by using cross-axis proportional gains. In *AIAA guidance, navigation, and control conference exhibit*, San Francisco, CA, August 2005, AIAA 2005–5955.
12. Hsu C-T and Chen S-L. Exact linearization of a voltage-controlled 3-pole active magnetic bearing system. *IEEE Trans Control Syst Technol* 2002; 10(4): 618–625.
13. Chen M and Knospe CR. Feedback linearization of active magnetic bearings: current-mode implementation. *IEEE/ASME Trans Mechatron* 2005; 10(6): 632–639.
14. Fang J and Ren Y. Decoupling control of a magnetically suspended rotor in a control moment gyro based on inverse system method. *IEEE/ASME Trans Mechatron* 2012; 17(6): 1133–1144.
15. Fang J and Ren Y. High-precision control for a single-gimbal magnetically suspended control moment gyro based on inverse system method. *IEEE Trans Ind Electron* 2011; 58(9): 4331–4342.
16. Dever TP, Brown GV, Duffy KP, et al. Modeling and development of a magnetic bearing controller for a high speed flywheel system. In: *Proceedings of 2nd international energy convers. engineering conference,* Providence, RI, August 2004, AIAA 2004–5626.
17. Wu F, Zhang X, Ju P, et al. Decentralized nonlinear control of wind turbine with doubly fed induction generator. *IEEE Trans Power Syst* 2008; 23(2): 613–621.
18. Lee T-S and Liu J-H. Modeling and control of a three-phase four-switch PWM voltage-source rectifier in d-q synchronous frame. *IEEE Trans Power Electron* 2011; 26(9): 2476–2489.
19. Ren Y and Fang J. Current-sensing resistor design to include current derivative in PWM H-bridge unipolar switching power amplifiers for magnetic bearings. *IEEE Trans Ind Electron* 2012; 59(12): 4590–4600.
20. Fan Y and Fang J. Experimental research on the nutational stability of magnetically suspended momentum flywheel in control moment gyroscope (CMG). In: *Proceedings of the 9th international. symposium on magnetic bearings*, Lexington, USA, August 2004.
21. Ren Y, Su D and Fang J. Whirling modes stability criterion for a magnetically suspended flywheel rotor with significant gyroscopic effects and bending modes. *IEEE Trans Power Electron* 2013; 28(12): 5890–5901. DOI: 10.1109/TPEL.2013.2253126.

Appendix 1

$$f(\boldsymbol{x}) = \begin{bmatrix} x_5 \\ x_6 \\ x_7 \\ x_8 \\ \dfrac{2k_{hby}l_m^2x_1 - H_{rz}\left(\frac{\sqrt{2}}{2}x_8\cos x_3 - \frac{\sqrt{2}}{2}x_7 + x_6\right) - \frac{\sqrt{2}}{2}J_{rr}\cos x_3\frac{\lambda_1 - \sqrt{2}l_m^2\left(k_{hby}x_1 + k_{hax}x_2\right)\cos x_3}{\lambda_2} \frac{\sqrt{2}}{2}J_{rr}x_7x_8\sin x_3 - \frac{\sqrt{2}}{2}J_{rr}\frac{\lambda_3 - \sqrt{2}l_m^2\left(k_{hby}x_1 - k_{hax}x_2\right)}{J_{gx}}}{J_{rr}} \\ \dfrac{2k_{hax}l_m^2x_2 + H_{rz}\left(\frac{\sqrt{2}}{2}x_8\cos x_3 + \frac{\sqrt{2}}{2}x_7 + x_5\right) - \frac{\sqrt{2}}{2}J_{rr}\cos x_3\frac{\lambda_1 - \sqrt{2}l_m^2\left(k_{hby}x_1 + k_{hax}x_2\right)\cos x_3}{\lambda_2} + \frac{\sqrt{2}}{2}J_{rr}x_7x_8\sin x_3 + \frac{\sqrt{2}}{2}J_{rr}\frac{\lambda_3 - \sqrt{2}l_m^2\left(k_{hby}x_1 - k_{hax}x_2\right)}{J_{gx}}}{J_{rr}} \\ \dfrac{\lambda_3 - \sqrt{2}l_m^2\left(k_{hby}x_1 - k_{hax}x_2\right)}{J_{gx}} \\ \dfrac{\lambda_1 - \sqrt{2}l_m^2\left(k_{hby}x_1 + k_{hax}x_2\right)\cos x_3}{\lambda_2} \end{bmatrix}$$

$$\boldsymbol{B}(\boldsymbol{x}) = \begin{bmatrix} \dfrac{2k_{hby}l_m^2x_1 - H_{rz}\left(\frac{\sqrt{2}}{2}x_8\cos x_3 - \frac{\sqrt{2}}{2}x_7 + x_6\right) - \frac{\sqrt{2}}{2}J_{rr}\cos x_3\frac{\lambda_1 - \sqrt{2}l_m^2\left(k_{hby}x_1 + k_{hax}x_2\right)\cos x_3}{\lambda_2} + \frac{\sqrt{2}}{2}J_{rr}x_7x_8\sin x_3 - \frac{\sqrt{2}}{2}J_{rr}\frac{\lambda_3 - \sqrt{2}l_m^2\left(k_{hby}x_1 - k_{hax}x_2\right)}{J_{gx}}}{J_{rr}} \\ \dfrac{2k_{hax}l_m^2x_2 + H_{rz}\left(\frac{\sqrt{2}}{2}x_8\cos x_3 + \frac{\sqrt{2}}{2}x_7 + x_5\right) - \frac{\sqrt{2}}{2}J_{rr}\cos x_3\frac{\lambda_1 - \sqrt{2}l_m^2\left(k_{hby}x_1 + k_{hax}x_2\right)\cos x_3}{\lambda_2} + \frac{\sqrt{2}}{2}J_{rr}x_7x_8\sin x_3 + \frac{\sqrt{2}}{2}J_{rr}\frac{\lambda_3 - \sqrt{2}l_m^2\left(k_{hby}x_1 - k_{hax}x_2\right)}{J_{gx}}}{J_{rr}} \\ \dfrac{\lambda_3 - \sqrt{2}l_m^2\left(k_{hby}x_1 - k_{hax}x_2\right)}{J_{gx}} \\ \dfrac{\lambda_1 - \sqrt{2}l_m^2\left(k_{hby}x_1 + k_{hax}x_2\right)\cos x_3}{\lambda_2} \end{bmatrix}$$

where $\lambda_1 = 2(J_{gy} - J_{gz})x_7x_8\sin x_3\cos x_3$ and $\lambda_3 = (J_{gz} - J_{gy})x_8^2\sin x_3\cos x_3$.

Appendix 2

Notation

f_{ax}	the magnetic forces along the radial magnetic coordinate Ax
f_{ay}	the magnetic forces along the radial magnetic coordinate Ay
f_{bx}	the magnetic forces along the radial magnetic coordinate Bx
f_{by}	the magnetic forces along the radial magnetic coordinate By
f_x	the magnetic forces in the X direction
f_y	the magnetic forces in Y direction
h_λ	the linear displacement of channel $\lambda(\lambda = ax, ay, bx, by)$
H_{rz}	the angular momentum of the MSR system
i_c	the feedback coefficient of the current-loop controller for the MSR system
i_λ	the winding current of channel $\lambda(\lambda = ax, ay, bx, by)$
J_{gx}	the moments of inertia along the X axes of the inner gimbal rate-servo system
J_{gy}	the moments of inertia along the Y axes of the inner gimbal rate-servo system
J_{gz}	the moments of inertia along the Z axes of the inner gimbal rate-servo system
J_{jy}	the moment of inertia in the output torque direction of the outer gimbal rate-servo system
J_{rr}	the moment of inertia along the radial magnetic coordinates of the MSR
J_z	the moment of inertia along the axial magnetic coordinates of the MSR
k_{am}	the proportional coefficient of the current-loop controller for the MSR system
k_f	the current-loop feedback coefficient of the gimbal servo systems.
k_{igx}	the current stiffness of the inner gimbal rate-servo system
k_{ijy}	the current stiffness of the outer gimbal rate-servo system
$k_{i\lambda}$	the current-force-factor of channel $\lambda(\lambda = ax, ay, bx, by)$
$k_{h\lambda}$	the displacement-force-factor of channel $\lambda(\lambda = ax, ay, bx, by)$
k_p	the current-loop proportional coefficient of the gimbal servo systems
m	the mass of the rotor
O	the geometric center of the magnetic bearing stator
p_{gx}	the output torque of the inner gimbal rate-servo system
p_{jy}	the output torque of the outer gimbal rate-servo system
p_x	the output torques in the X direction
p_y	the output torques in the Y directions
α	the rotational angle about the X axes
β	the rotational angle about the Y axes
θ_g	the rotational angles of the inner gimbal
θ_j	the rotational angles of the outer gimbal
ε_1	the parameters of the IMC
ε_2	the parameters of the IMC
Ω	the rotor speed